TRIANGULAR-GRID BILLIARDS AND PLABIC GRAPHS

Colin Defant*[1] and Pakawut Jiradilok†[2]

[1,2]*Department of Mathematics, Massachusetts Institute of Technology, Cambridge, MA 02139, U.S.A.*
colindefant@gmail.com , pakawut@mit.edu

Submitted: Mar 14, 2022; Accepted: Nov 19, 2022; Published: Mar 15, 2023

Abstract. Given a polygon P in the triangular grid, we obtain a permutation π_P via a natural billiards system in which beams of light bounce around inside of P. The different cycles in π_P correspond to the different trajectories of light beams. We prove that

$$\operatorname{area}(P) \geqslant 6\operatorname{cyc}(P) - 6 \quad \text{and} \quad \operatorname{perim}(P) \geqslant \frac{7}{2}\operatorname{cyc}(P) - \frac{3}{2},$$

where $\operatorname{area}(P)$ and $\operatorname{perim}(P)$ are the (appropriately normalized) area and perimeter of P, respectively, and $\operatorname{cyc}(P)$ is the number of cycles in π_P. The inequality concerning $\operatorname{area}(P)$ is tight, and we characterize the polygons P satisfying $\operatorname{area}(P) = 6\operatorname{cyc}(P) - 6$. These results can be reformulated in the language of Postnikov's plabic graphs as follows. Let G be a connected reduced plabic graph with essential dimension 2. Suppose G has n marked boundary points and v (internal) vertices, and let c be the number of cycles in the trip permutation of G. Then we have

$$v \geqslant 6c - 6 \quad \text{and} \quad n \geqslant \frac{7}{2}c - \frac{3}{2}.$$

Keywords. Triangular grid, billiards, plabic graph, membrane
Mathematics Subject Classifications. 05D99, 51M04

1. Introduction

1.1. Triangular grid billiards

Consider the infinite triangular grid in the plane, scaled so that each equilateral triangular grid cell has side length 1 and oriented so that some of the grid lines are horizontal. We refer to the

*Supported by the National Science Foundation under Award No. DGE–1656466 and Award No. 2201907, by a Fannie and John Hertz Foundation Fellowship, and by a Benjamin Peirce Fellowship at Harvard University.
†Supported by Elchanan Mossel's Vannevar Bush Faculty Fellowship ONR-N00014-20-1-2826 and Elchanan Mossel's Simons Investigator award (622132).

sides of these grid cells as *panes* because we will imagine that each pane either allows light to pass through it (like a window pane) or reflect off of it (like a mirror pane). Define a *grid polygon* to be a (not necessarily convex) polygon whose boundary is a union of panes. We assume that the boundary of a grid polygon (viewed as a closed curve) does not intersect itself. Suppose P is a grid polygon whose boundary panes are $b_1, \dots, b_n$, listed clockwise. Pick some boundary pane b_i, and emit a colored beam of light from the midpoint of b_i into the interior of P so that the light beam forms a 60° angle with b_i and travels either northeast, southeast, or west (depending on the orientation of b_i). The light beam will travel through the interior of P until reaching the midpoint of a different boundary pane $b_{\pi(i)}$, which it will meet at a 60° angle. This defines a permutation $\pi = \pi_P \colon [n] \to [n]$ (where $[n] := \{1, \dots, n\}$) called the *billiards permutation* of P. For example, if P is the grid polygon in Figure 1.1, then the cycle decomposition of π_P is

$$(1\,3\,32\,26\,6\,30\,2\,33\,25\,12\,14\,9\,21\,19\,29\,28\,4\,31)(5\,24\,13\,10\,20\,27)(7\,22\,23\,15\,17)(8\,11\,18\,16).$$

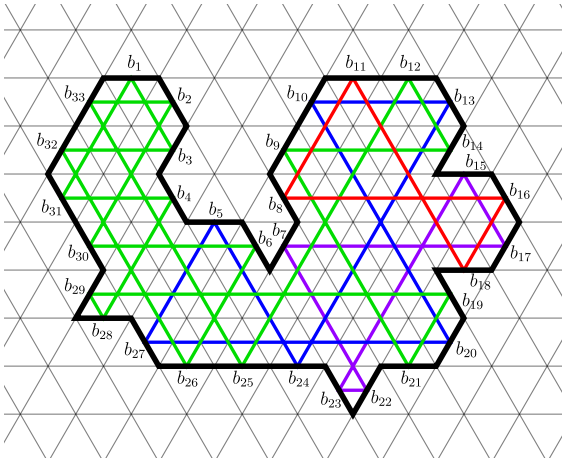

Figure 1.1: A grid polygon P with 33 boundary panes. The billiards permutation π_P has 4 cycles. We have colored the 4 different trajectories with different colors.

One can interpret this definition of π as a certain billiards process. Let us imagine that the boundary panes of P are mirrors (and all other panes are transparent windows). When the light beam emitted from b_i reaches $b_{\pi(i)}$, it will bounce off in such a way that the reflected beam forms a 60° angle with $b_{\pi(i)}$. This reflected beam will then travel to $b_{\pi^2(i)}$, where it will bounce off at a 60° angle and continue on to $b_{\pi^3(i)}$, and so on. We will be interested in the cycles of π. Given points p and p' in the plane, let us write $[p, p']$ for the line segment whose endpoints are p and p'. Let $\mathrm{mid}(s)$ denote the midpoint of a line segment s. If $c = (i_1\, i_2 \cdots i_r)$ is a cycle of π, then we define the *trajectory* of c to be

$$\mathrm{traj}(c) = \bigcup_{j=1}^{r} [\mathrm{mid}(b_{i_j}), \mathrm{mid}(b_{\pi(i_j)})].$$

The description of π in terms of light beam billiards is convenient because we can imagine that the beams of light corresponding to different cycles have different colors; thus, we will use different colors to draw different trajectories (see Figure 1.1).

The investigation of billiards in planar regions is a classical and much-beloved topic in both dynamical systems and recreational mathematics [BKM78, CFG91, CSD63, DR85, DR83, Gar84, Gut86, Hal77, SK79]. However, the typical questions considered in previous works concern systems where the beams of light can have arbitrary initial positions and arbitrary initial directions. In contrast, our setup—which surprisingly appears to be new—imposes a great deal of rigidity by requiring each beam of light to start at the midpoint of a boundary pane and begin its journey in a direction that forms a 60° angle with that boundary pane. Although several traditional dynamically-flavored billiards problems (such as determining the existence of periodic trajectories) become trivial or meaningless under our rigid conditions, our setting affords some fascinating combinatorial/geometric questions.

The major players in our story are the following quantities associated with a grid polygon P. The *perimeter* of P, denoted $\mathrm{perim}(P)$, is simply the number of boundary panes of P. We define the *area* of P, denoted $\mathrm{area}(P)$, to be the number of triangular grid cells in P.[1] We write $\mathrm{cyc}(P)$ for the number of cycles in the associated permutation π_P, which is the same as the number of different light beam trajectories in the associated billiards system. Our main theorems address the following extremal question concerning the possible relationships between these quantities: How big must $\mathrm{area}(P)$ and $\mathrm{perim}(P)$ be in comparison with $\mathrm{cyc}(P)$?

Theorem 1.1. *If P is a grid polygon, then*

$$\mathrm{area}(P) \geqslant 6\,\mathrm{cyc}(P) - 6.$$

Theorem 1.2. *If P is a grid polygon, then*

$$\mathrm{perim}(P) \geqslant \frac{7}{2}\,\mathrm{cyc}(P) - \frac{3}{2}.$$

The inequality in Theorem 1.1 is tight, and we will characterize the grid polygons that achieve equality. Define a *unit hexagon* to be a grid polygon that is a regular hexagon of side length 1. Let us construct a sequence of grid polygons $(P_k)_{k\geqslant 1}$ as follows. First, let P_1 be a unit hexagon. For $k \geqslant 2$, let $P_k = P_{k-1} \cup Q_k$, where Q_k is a unit hexagon such that $P_{k-1} \cap Q_k$ is a single pane. We call a grid polygon P_k obtained in this manner a *tree of unit hexagons*; see Figure 1.2 for an example with $k = 9$. Since $\mathrm{cyc}(Q_k) = 2$ for all $k \geqslant 2$, one can combine Corollary 3.2 from below with an easy inductive argument to see that $\mathrm{cyc}(P_k) = k + 1$ for all $k \geqslant 1$. Thus, $\mathrm{area}(P_k) = 6k = 6\,\mathrm{cyc}(P_k) - 6$.

Theorem 1.3. *If P is a grid polygon, then $\mathrm{area}(P) = 6\,\mathrm{cyc}(P) - 6$ if and only if P is a tree of unit hexagons.*

On the other hand, we believe that Theorem 1.2 is not tight. After drawing several examples of grid polygons, we have arrived at the following conjecture.

[1] Thus, our area measure is just the Euclidean area multiplied by the normalization factor $4/\sqrt{3}$.

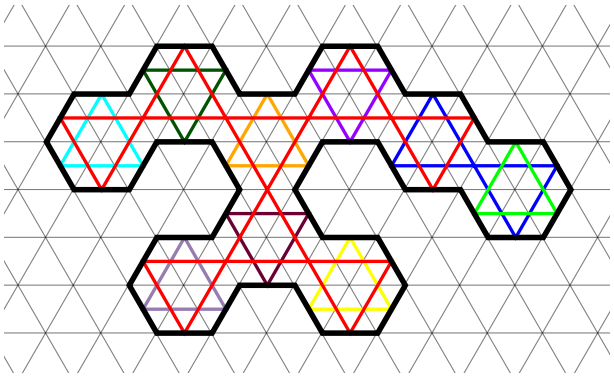

Figure 1.2: A tree of unit hexagons P_9 with $\mathrm{cyc}(P_9) = 10$, $\mathrm{area}(P_9) = 54$, and $\mathrm{perim}(P_9) = 38$.

Conjecture 1.4. If P is a grid polygon, then

$$\mathrm{perim}(P) \geqslant 4\,\mathrm{cyc}(P) - 2.$$

If Conjecture 1.4 is true, then it is tight. Indeed, if P_k is a tree of unit hexagons as described above, then $\mathrm{perim}(P_k) = 4k + 2 = 4\,\mathrm{cyc}(P_k) - 2$.

Of fundamental importance in our analysis of the billiards system of a grid polygon P are the *triangular trajectories* of P, which are just the trajectories of the 3-cycles in π_P. One of the crucial ingredients in the proofs of Theorems 1.1–1.3 is the following result, which we deem to be noteworthy on its own.

Theorem 1.5. *Let P be a grid polygon, and let c be a cycle of size m in π_P. Then the trajectory $\mathrm{traj}(c)$ intersects at most $m - 2$ triangular trajectories of P (excluding $\mathrm{traj}(c)$ itself if $m = 3$).*

1.2. Plabic graphs

A *plabic graph* is a planar graph G embedded in a disc such that each vertex is colored either black or white. We assume that the boundary of the disc has n marked points labeled clockwise as $b_1^*, \ldots, b_n^*$ so that each b_i^* is connected via an edge to exactly one vertex of G. Following [LP20], we will also assume that every vertex of G is incident to exactly 3 edges, including edges connected to the boundary of the disc (the study of general plabic graphs can be reduced to this case). In his seminal article [Pos06], Postnikov introduced plabic graphs—along with several other families of combinatorial objects—in order to parameterize cells in the totally nonnegative Grassmannian. These graphs have now found remarkable applications in a variety of fields such as cluster algebras, knot theory, polyhedral geometry, scattering amplitudes, and shallow water waves [AHBC+16, FPST22, GPW22, KW14, LP20, LPW20, PSBW21, STWZ19].

Imagine starting at a marked boundary point b_i^* and traveling along the unique edge connected to b_i^*. Each time we reach a vertex, we follow the *rules of the road* by turning right if the vertex is black and turning left if the vertex is white. Eventually, we will reach a marked boundary point $b_{\pi(i)}^*$. The path traveled is called the *trip* starting at b_i^*. Considering the trips starting at all of the different marked boundary points yields a permutation $\pi = \pi_G : [n] \to [n]$ called the *trip*

permutation of G. We say G is *reduced* if it has the minimum number of faces among all plabic graphs with the same trip permutation. Figure 1.3 shows a reduced plabic graph G whose trip permutation is the cycle $\pi_G = (1\,3\,5\,2\,4)$.

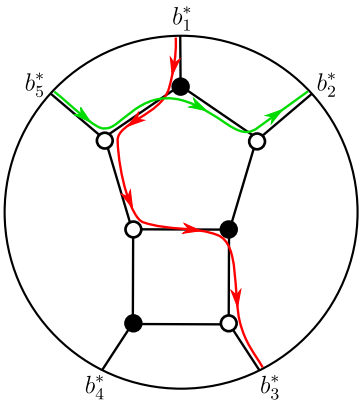

Figure 1.3: A reduced plabic graph whose trip permutation is the cycle $(1\,3\,5\,2\,4)$. The fact that $\pi_G(1) = 3$ is illustrated by the red trip starting at b_1^* and ending at b_3^*. Similarly, $\pi_G(5) = 2$ because the green trip starting at b_5^* ends at b_2^*.

Given a grid polygon P, one can obtain a reduced plabic graph $G(P)$ via a planar dual construction. Let us say an equilateral triangle with a horizontal side is *right-side up* (respectively, *upside down*) if its horizontal side is on its bottom (respectively, top). We refer to this property of a triangle (right-side up or upside down) as its *orientation*. Place a black (respectively, white) vertex at the center of each right-side up (respectively, upside down) equilateral triangular grid cell inside of P. Whenever two such grid cells share a side, draw an edge between the corresponding vertices. Finally, encompass P in a disc, draw a marked point b_i^* on the boundary of the disc corresponding to each boundary pane b_i of P, and draw an edge from b_i^* to the vertex drawn inside the unique grid cell that has b_i as a side. See Figure 1.4.

It is immediate from the relevant definitions that the trip permutation $\pi_{G(P)}$ is equal to the billiards permutation π_P. For example, if P and $G(P)$ are as in Figure 1.4, then $\pi_P = \pi_{G(P)}$ is the permutation with cycle decomposition $(1\,7\,4\,3\,5\,9)(2\,6\,8)$.

1.3. Membranes

In the recent paper [LP20], Lam and Postnikov introduced *membranes*, which are certain triangulated 2-dimensional surfaces embedded in a Euclidean space. The definition of a membrane relies on a choice of an irreducible root system, and most of the discussion in [LP20] centers around membranes of type A. They discussed how type A membranes are in a sense dual to plabic graphs, and they further related type A membranes to the theory of cluster algebras. A membrane is *minimal* if it has the minimum possible surface area among all membranes with the same boundary; Lam and Postnikov showed how to associate a reduced plabic graph $G(M)$ to each minimal type A membrane M. They then defined the *essential dimension* of a reduced

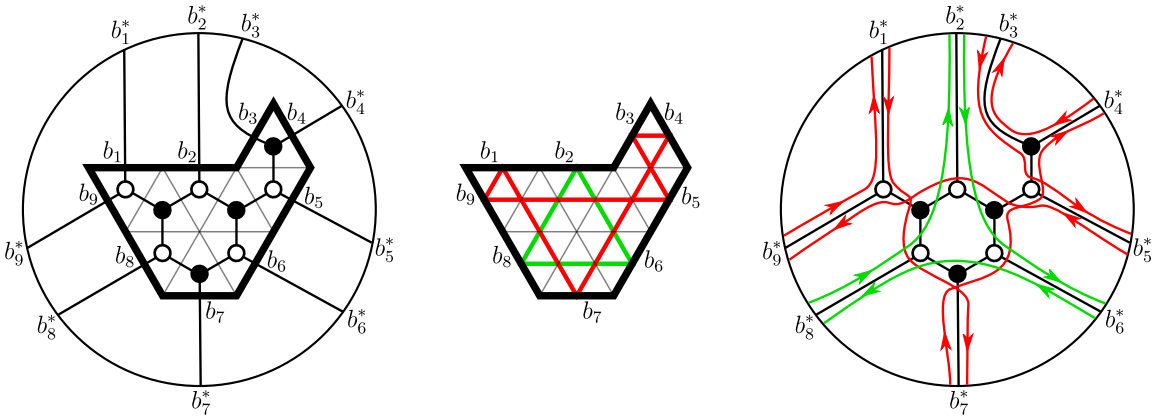

Figure 1.4: On the left is a grid polygon P overlaid with the corresponding plabic graph $G(P)$. The middle image shows the trajectories in the billiards system of P to illustrate that its billiards permutation is $\pi_P = (1\,7\,4\,3\,5\,9)(2\,6\,8)$. The right image shows the trips of $G(P)$ to illustrate that its trip permutation is $\pi_{G(P)} = (1\,7\,4\,3\,5\,9)(2\,6\,8)$.

plabic graph G_0 to be the smallest positive integer d such that there exists a minimal membrane M of type A_d with $G(M) = G_0$. They proved that if G_0 has n marked boundary points, then the essential dimension of G_0 is at most $n-1$, with equality holding if and only if there exists $k \in [n-1]$ such that $\pi_{G_0}(i) = i + k \pmod n$ for all $i \in [n]$ (this is equivalent to saying that G_0 corresponds to the top cell in the totally nonnegative Grassmannian $\mathrm{Gr}_{k,n}^{\geqslant 0}$). Other than this result, there is essentially nothing known about essential dimensions of plabic graphs. Our original motivation for this project was to initiate the investigation of essential dimensions by studying plabic graphs of essential dimension 2 in detail.

Consider the class of triangulated surfaces in the triangular grid that can be obtained by iteratively wedging grid polygons. In other words, Q is in this class if there are grid polygons $P_1, \ldots, P_k$ such that $P_{i+1} \cap (P_1 \cup \cdots \cup P_i)$ is a single point for all $i \in [k-1]$ and such that $Q = P_1 \cup \cdots \cup P_k$. In this case, we call the grid polygons $P_1, \ldots, P_k$ the *components* of Q. See Figure 1.5. As mentioned in [LP20], the class we have just described is the same as the class of membranes of type A_2. Such a membrane M is automatically minimal (since it is determined by its boundary). In order to understand these membranes and their associated reduced plabic graphs, it suffices to understand grid polygons and their associated reduced plabic graphs. Indeed, the reduced plabic graphs associated to the components of M are basically the same as the connected components of the reduced plabic graph associated to M; thus, restricting our focus to grid polygons is the same as restricting our focus to connected plabic graphs. Furthermore, if $M = P$ is a grid polygon, then the definition that Lam and Postnikov gave for the reduced plabic graph $G(M)$ associated to M (viewed as a membrane) is exactly the same as the definition that we gave in Section 1.2 for the reduced plabic graph $G(P)$ associated to P (viewed as a grid polygon). In other words, understanding plabic graphs of essential dimension 2 and their trip permutations is equivalent to understanding grid polygons and their billiards permutations.

As a consequence of the preceding discussion, we can reformulate Theorems 1.1 and 1.2 in

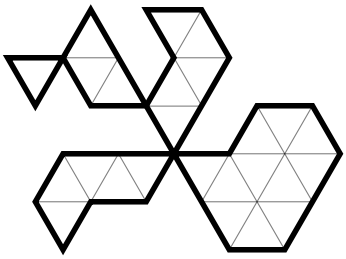

Figure 1.5: A membrane of type A_2 with 5 components.

the language of plabic graphs.

Corollary 1.6. *Let G be a connected reduced plabic graph with essential dimension 2. Suppose G has n marked boundary points and v vertices, and let c be the number of cycles in the trip permutation π_G. Then*

$$v \geqslant 6c - 6 \quad \textit{and} \quad n \geqslant \frac{7}{2}c - \frac{3}{2}.$$

Proof. By the preceding discussion, there is a grid polygon P such that $G = G(P)$. We have $\mathrm{perim}(P) = n$, $\mathrm{area}(P) = v$, and $\mathrm{cyc}(P) = c$, so the corollary follows from Theorems 1.1 and 1.2. □

1.4. Outline

Section 2 is devoted to the proof of Theorem 1.5. In Section 3, we apply Theorem 1.5 to prove Theorems 1.1, 1.2, and 1.3. We believe that our work opens the door to several new combinatorial and geometric questions; we have collected many ideas for future work in Section 4.

2. Triangles intersecting a trajectory

Our goal in this section is to prove Theorem 1.5. We begin with a lemma that establishes this theorem in the special case when $m = 3$.

Lemma 2.1. *Suppose Δ is a triangular trajectory in the billiards system of a grid polygon P. There is at most one triangular trajectory Δ' in P that intersects Δ and is not equal to Δ. If such a trajectory Δ' exists, then its orientation must be opposite to that of Δ.*

Proof. If two triangular trajectories intersect, then neither one can have a vertex in the interior of the region bounded by the other. This forces the two triangular trajectories to have opposite orientations. It also implies that every side of the first trajectory intersects the second trajectory and vice versa (i.e., the trajectories intersect in 6 points). It follows from these observations that a triangular trajectory cannot intersect two other triangular trajectories. □

Let us fix some additional notation and terminology concerning trajectories. When we refer to a *line segment*, we assume by default that it contains its endpoints and that it is not a single point. Let P be a grid polygon, and let c be an m-cycle in π_P. Since Lemma 2.1 tells us that Theorem 1.5 is true when $m = 3$, we will assume that $m \geqslant 4$. Let $z_1, \dots, z_m$ be the points where the trajectory $\mathrm{traj}(c)$ intersects the boundary of P, listed clockwise around the boundary. For convenience, let $z_{m+1} = z_1$. Imagine traversing the boundary of P clockwise, and let B_i be the part of the boundary traversed between z_i and z_{i+1}, including z_i and z_{i+1}. We call each B_i a *shoreline* of $\mathrm{traj}(c)$. Note that $\mathrm{traj}(c)$ is the union of m line segments, each of which has its endpoints in $\{z_1, \dots, z_m\}$. Let C be the set of points where two of these line segments intersect each other (including $z_1, \dots, z_m$). If we "cut" $\mathrm{traj}(c)$ at each point in C, we will break each of the m line segments into smaller line segments that we call the *fragments* of $\mathrm{traj}(c)$. More precisely, we say a line segment $f \subseteq \mathrm{traj}(c)$ is a *fragment* of $\mathrm{traj}(c)$ if the endpoints of f belong to C and if the relative interior of f does not contain any points from C. We say a fragment f *sees* a shoreline B if there exist a point p in the relative interior of f and a point p' in B that is not an endpoint of B such that the relative interior of the line segment $[p, p']$ lies inside of P and does not contain any points from $\mathrm{traj}(c)$. If f is a fragment of $\mathrm{traj}(c)$ that sees the shoreline B, then we write $E(f, B)$ for the equilateral triangle that has f as one of its sides and that lies on the side of f opposite to B. See Figure 2.1.

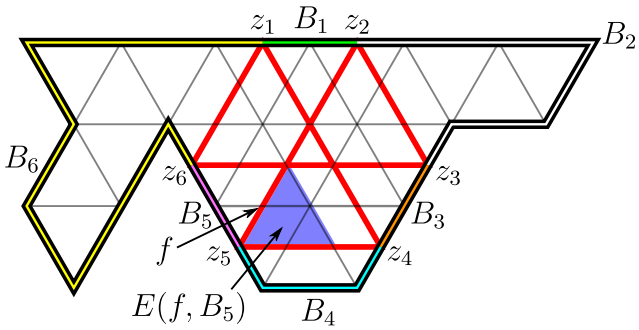

Figure 2.1: In red is the trajectory of a 6-cycle in the billiards system of a grid polygon. This trajectory has 12 fragments. The 6 shorelines are represented with different colors. Each of B_1, B_3, B_5 is seen by exactly 2 of the fragments, while each of B_2, B_4, B_6 is seen by exactly 1 of the fragments. We have labeled one of the fragments f that sees B_5, and we have shaded the triangle $E(f, B_5)$ in blue.

Fix a shoreline B, and let $f_1, \dots, f_k$ be the fragments of $\mathrm{traj}(c)$ that see B. Then $f_1 \cup \cdots \cup f_k \cup B$ is a piecewise-linear curve that bounds a polygonal region R. Let us assume that $f_1, \dots, f_k$ are listed in clockwise order around R so that f_1 and f_k touch B. For each $j \in [k-1]$, let θ_j be the interior angle of R at the point of intersection of f_j and f_{j+1}. It is straightforward to see that θ_j is either 60° or 120°. Let $K = K(B) = 1 + \sum_{j=1}^{k-1} \beta_j$, where $\beta_j = 2$ if $\theta_j = 60^\circ$ and $\beta_j = 1$ if $\theta_j = 120^\circ$. A schematic illustration of this situation is shown in Figure 2.3. In that figure, we have $\theta_1 = \theta_3 = 120^\circ$ and $\theta_2 = 60^\circ$, so $\beta_1 = \beta_3 = 1$, $\beta_2 = 2$, and $K(B) = 1 + (1 + 2 + 1) = 5$.

Imagine standing at the point $B \cap f_k$ and facing toward B. Walk along the shoreline B to reach $B \cap f_1$; you should now be facing toward the shoreline that comes immediately after B in clockwise order. The net change in your direction during this walk is $(180 - 60K)^\circ$ clockwise.[2] To see this, consider instead walking from $B \cap f_k$ to $B \cap f_1$ by traversing the fragments $f_k, \ldots, f_1$; this will result in the same net change in direction. You first turn 60° clockwise to get onto the fragment f_k. Whenever you transfer from f_{j+1} to f_j, you turn $(180^\circ - \theta_j) = (60\beta_j)^\circ$ counterclockwise, which is the same as $(-60\beta_j)^\circ$ clockwise. At the end, you turn another 60° clockwise to get off of f_1 and face toward the next shoreline. Overall, your net change in direction is $60^\circ + \sum_{j=1}^{k-1}(-60\beta_j)^\circ + 60^\circ = (180 - 60K)^\circ$ clockwise. In the example shown in Figure 2.3, the net change of direction would be $60^\circ - 60^\circ - 120^\circ - 60^\circ + 60^\circ = -120^\circ = (180 - 60K)^\circ$ clockwise (i.e., 120° counterclockwise).

We are going to prove that the number of triangular trajectories that intersect $\mathrm{traj}(c)$ and touch B is at most K. First, we need the following lemmas.

Lemma 2.2. *Preserve the notation from above. For each $i \in [k]$, the boundary of the grid polygon P does not intersect the interior of $E(f_i, B)$.*

Proof. Without loss of generality, we may assume that $E(f_i, B)$ is right-side up and has f_i as its (horizontal) bottom side. Let $\mathcal{W}$ denote the intersection of the boundary of P and the interior of $E(f_i, B)$. Suppose for the sake of contradiction that $\mathcal{W}$ is nonempty. It is not hard to see that there is a point $w^* \in \mathcal{W}$ whose distance to f_i is the minimum among all points in $\mathcal{W}$. Let T_{w^*} be the unique equilateral triangle that contains w^* as a vertex and has one of its sides contained in f_i. By the minimality of the distance from w^* to f_i, we observe that T_{w^*} does not contain other points from the boundary of P besides w^*. See Figure 2.2.

Note that the space $P \setminus (R \cup T_{w^*})$ has two connected components: a left region whose closure contains the left endpoint of f_i and a right region whose closure contains the right endpoint of f_i. Imagine following the trajectory $\mathrm{traj}(c)$ starting at the right endpoint of f_i and continuing through the left endpoint of f_i. You will land in the left region. If you continue following the trajectory, you will eventually come back to the right endpoint of f_i, which is in the right region. Since $\mathrm{traj}(c)$ does not intersect the interior of R, it must travel from the left region to the right region through T_{w^*}. However, this means that there exists a horizontal boundary pane of P inside T_{w^*}, which is a contradiction. □

Lemma 2.3. *Preserve the notation from above. If a triangular trajectory intersects $\mathrm{traj}(c)$ and touches B, then it touches B at exactly 1 point.*

Proof. Let Δ be a triangular trajectory that intersects $\mathrm{traj}(c)$ and touches B. Let f be a fragment of $\mathrm{traj}(c)$ that intersects Δ. Let a_1, a_2, a_3 be the vertices of Δ. It is easy to see that Δ cannot have all 3 of its vertices on B. Now suppose Δ has exactly 2 of its vertices, say a_1 and a_2, on B. By rotating P if necessary, we may assume $[a_1, a_2]$ is a horizontal line segment. The boundary of P does not pass through the interior of the region bounded by Δ; combining this with the observation that $\mathrm{traj}(c)$ does not intersect $[a_1, a_2]$; we find that every fragment of $\mathrm{traj}(c)$

[2] A net change of, say, 120° clockwise is different from a net change of -240° clockwise. In the former case, you spun 120° clockwise; in the latter case, you spun 240° counterclockwise.

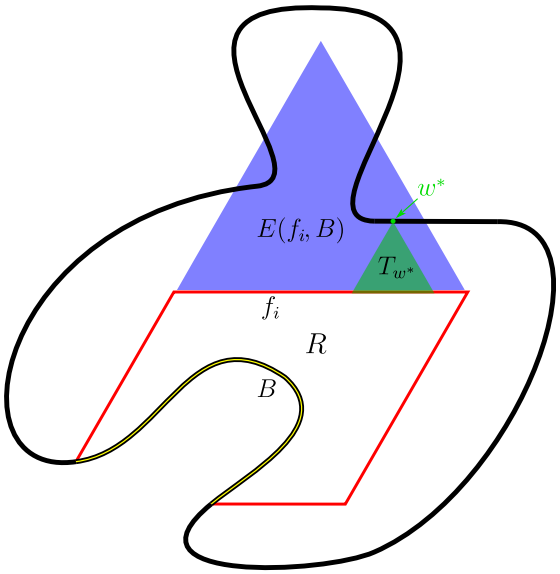

Figure 2.2: In this schematic drawing, the boundary of P passes through the interior of $E(f_i, B)$, where B is the shoreline indicated by a thin yellow strip and f_i is a fragment that sees B. The proof of Lemma 2.2 derives a contradiction from this setup.

passing through the interior of the region bounded by Δ must be horizontal. It follows that f is a horizontal line segment that intersects $[a_1, a_3]$ and $[a_2, a_3]$. However, this forces a_3 to be in the interior of $E(f, B)$, contradicting Lemma 2.2. □

Lemma 2.4. *Preserve the notation from above. There are at most $K(B)$ triangular trajectories in the billiards system of P that intersect $\mathrm{traj}(c)$ and touch B.*

Proof. We illustrate the proof in Figure 2.3. For each $i \in [k]$ and each side s of the triangle $E(f_i, B)$, it follows from Lemma 2.2 that there is a unique line segment $L(s)$ containing s that does not pass through the exterior of P and whose endpoints are on the boundary of P. Let

$$X = \bigcup_{i=1}^{k} \bigcup_{\substack{s \text{ a side} \\ \text{of } E(f_i,B)}} L(s).$$

Define an *X-region* to be the closure of a connected component of $P \setminus X$; let $\mathcal{R}_X$ be the set of X-regions. Say an X-region V is *hospitable* if it contains at least one side of at least one of the triangles $E(f_1, B), \dots, E(f_k, B)$; otherwise, say V is *inhospitable*. Then $E(f_1, B), \dots, E(f_k, B)$ are k different hospitable X-regions. It is straightforward to see that an X-region is of the form $E(f_i, B)$ for some $i \in [k]$ if and only if it does not contain a line segment in the boundary of P. Let R be the X-region whose boundary is $f_1 \cup \cdots \cup f_k \cup B$. Let R' (respectively, R'') be the unique X-region other than R that contains the point $f_1 \cap B$ (respectively, $f_k \cap B$). Note that R, R', and R'' are hospitable. One can readily check that there are exactly $K(B) - 1$ hospitable X-regions in $\mathcal{R}_X \setminus \{E(f_1, B), \dots, E(f_k, B), R, R', R''\}$; let $U_1, \dots, U_{K(B)-1}$ be these X-regions. Finally, let $I_1, \dots, I_\ell$ be the inhospitable X-regions.

Let t be the number of triangular trajectories that intersect $\mathrm{traj}(c)$ and touch B, and let $p_1, \dots, p_{3t}$ be the points where these triangular trajectories touch the boundary of P. For each X-region V, let $g(V) = |V \cap \{p_1, \dots, p_{3t}\}|$. Each of the points $p_1, \dots, p_{3t}$ belongs to exactly one X-region, so $\sum_{V \in \mathcal{R}_X} g(V) = 3t$. It follows from Lemma 2.3 that $g(R) = t$. Lemma 2.2 immediately implies that $g(E(f_i, B)) = 0$ for all $i \in [k]$. Furthermore, using Lemma 2.2, one can readily check that $g(R') \leqslant 1$, $g(R'') \leqslant 1$, $g(U_j) \leqslant 2$ for all $j \in [K(B) - 1]$, and $g(I_h) = 0$ for all $h \in [\ell]$. Thus,

$$3t = \sum_{V \in \mathcal{R}_X} g(V) \leqslant t + 1 + 1 + \sum_{i=1}^{k} 0 + \sum_{j=1}^{K(B)-1} 2 + \sum_{h=1}^{\ell} 0 = t + 2K(B).$$

Hence, $t \leqslant K(B)$. □

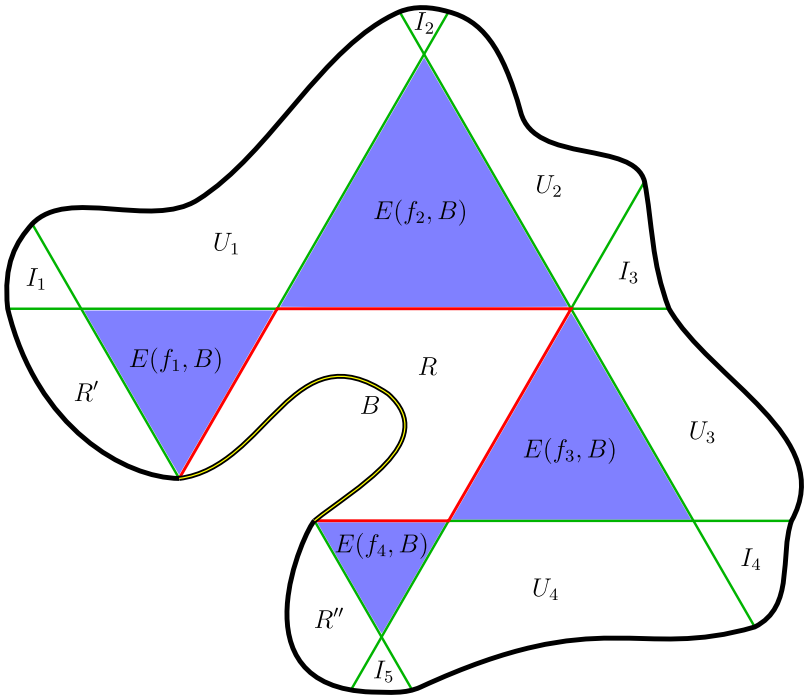

Figure 2.3: A schematic illustration of the proof of Lemma 2.4. The curvy black curve is meant to represent the boundary of P. The red line segments are the fragments f_1, f_2, f_3, f_4, and the shoreline B is marked with a thin yellow strip. The set X is the union of the red and green line segments. In this example, $K(B) = 5$.

We are now in a position to complete the proof of Theorem 1.5.

Proof of Theorem 1.5. Let P be a grid polygon, and let c be an m-cycle in π_P. If $m = 3$, then Theorem 1.5 follows from Lemma 2.1, so we may assume $m \geqslant 4$. Let $B_1, \dots, B_m$ be the shorelines of $\mathrm{traj}(c)$. For each shoreline B_i, we define the integer $K(B_i)$ as above. Lemma 2.4 tells

us that there are at most $K(B_i)$ triangular trajectories that intersect $\mathrm{traj}(c)$ and touch B_i, and Lemma 2.3 tells us that each such triangular trajectory touches B_i in exactly 1 point. Therefore, the total number of points where the triangular trajectories that intersect $\mathrm{traj}(c)$ touch the boundary of P is at most $\sum_{i=1}^m K(B_i)$. Since each triangular trajectory touches the boundary of P in exactly 3 points, we deduce that the total number of triangular trajectories that intersect $\mathrm{traj}(c)$ is at most $\frac{1}{3}\sum_{i=1}^m K(B_i)$. Hence, the proof will be complete if we can show that $\frac{1}{3}\sum_{i=1}^m K(B_i) = m-2$.

Preserve the notation from above. Imagine traversing the boundary of P clockwise, starting and ending at z_1. We saw in our discussion above that the net change in your direction when you traverse the shoreline B_i is $(180 - 60K(B_i))^\circ$ clockwise. Thus, the net change in your direction when you traverse the entire boundary of P is $\sum_{i=1}^m (180-60K(B_i))^\circ$ clockwise. But this net change must be 360°, so $\sum_{i=1}^m (180 - 60K(B_i)) = 360$. Manipulating this equation yields $\frac{1}{3}\sum_{i=1}^m K(B_i) = m-2$, as desired. □

3. Areas and perimeters

We will find it useful to break grid polygons into smaller grid polygons; the following lemma allows us to understand the effect that this has on the enumeration of the cycles in the associated billiards systems.

Lemma 3.1. *Let P be a grid polygon, and suppose $P = P_1 \cup P_2$, where P_1 and P_2 are grid polygons such that $P_1 \cap P_2$ is a union of η different panes. Let δ_i be the number of different trajectories in the billiards system of P_i that touch $P_1 \cap P_2$. Then*

$$\mathrm{cyc}(P) \leqslant \mathrm{cyc}(P_1) + \mathrm{cyc}(P_2) - \delta_1 - \delta_2 + \eta.$$

Proof. For each $i \in \{1,2\}$, the billiards system of P_i contains $\mathrm{cyc}(P_i) - \delta_i$ trajectories that do not touch $P_1 \cap P_2$, and these are also trajectories in the billiards system of P. It is straightforward to see that the billiards system of P has at most η trajectories that intersect $P_1 \cap P_2$. □

If $\eta = 1$ in the preceding lemma, then $\delta_1 = \delta_2 = 1$, and there must be exactly one trajectory in the billiards system of P that intersects $P_1 \cap P_2$. Hence, we have the following useful corollary.

Corollary 3.2. *Let $P = P_1 \cup P_2$, where P_1 and P_2 are grid polygons such that $P_1 \cap P_2$ is a single pane. Then* $\mathrm{cyc}(P) = \mathrm{cyc}(P_1) + \mathrm{cyc}(P_2) - 1$.

Let us say a grid polygon P is *primitive* if there do not exist grid polygons P_1 and P_2 such that $P = P_1 \cup P_2$ and such that $P_1 \cap P_2$ is a single pane. Corollary 3.2 will allow us to restrict our attention to primitive grid polygons. We will often need to handle the grid polygons in Figure 3.1 (and their rotations) separately. The proof of the next lemma is the main place where we apply Theorem 1.5, which we proved in Section 2.

Lemma 3.3. *Let P be a primitive grid polygon that is not a rotation of one of the grid polygons in Figure 3.1. Let α_m be the number of m-cycles in π_P. Then $\alpha_3 \leqslant \alpha_4 + \sum_{m \geqslant 5} (m-2)\alpha_m$.*

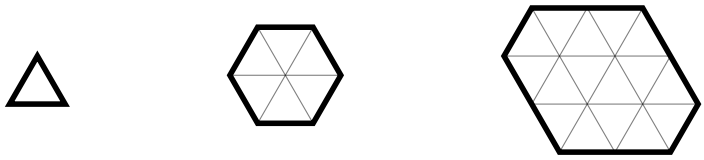

Figure 3.1: Three primitive grid polygons.

Proof. For each 3-cycle c in π_P, let $F(c)$ be the set of cycles in π_P whose trajectories intersect $\mathrm{traj}(c)$. Let Y be the set of 3-cycles c in π_P such that $F(c)$ contains only 3-cycles and 4-cycles. Using the hypothesis that P is primitive and not a rotation of one of the polygons in Figure 3.1, it is straightforward (though somewhat tedious) to verify if $c \in Y$, then $F(c)$ contains at least two 4-cycles. On the other hand, Theorem 1.5 tells us that if d is a 4-cycle in π_P, then there are at most two 3-cycles c in Y with $d \in F(c)$. Therefore, $|Y| \leqslant \alpha_4$.

If c is a 3-cycle in π_P that is not in Y, then $F(c)$ contains at least one cycle of size at least 5. Theorem 1.5 tells us that if d is an m-cycle in π_P, then there are at most $m-2$ different 3-cycles c such that $d \in F(c)$. This implies that $\alpha_3 - |Y| \leqslant \sum_{m\geqslant 5}(m-2)\alpha_m$. □

We can now prove our main theorem concerning perimeters of grid polygons.

Proof of Theorem 1.2. The result is trivial if $\mathrm{area}(P) = 1$, so we may assume $\mathrm{area}(P) \geqslant 2$ and proceed by induction on $\mathrm{area}(P)$. If P is not primitive, then we can write $P = P_1 \cup P_2$, where P_1 and P_2 are smaller grid polygons such that $P_1 \cap P_2$ is a single pane. By induction, we have $\mathrm{perim}(P_i) \geqslant \frac{7}{2}\,\mathrm{cyc}(P_i) - \frac{3}{2}$ for each $i \in \{1,2\}$. Combining this with Corollary 3.2 yields

$$\mathrm{perim}(P) = \mathrm{perim}(P_1) + \mathrm{perim}(P_2) - 2 \geqslant \frac{7}{2}(\mathrm{cyc}(P_1) + \mathrm{cyc}(P_2) - 1) - \frac{3}{2} = \frac{7}{2}\,\mathrm{cyc}(P) - \frac{3}{2},$$

as desired. Hence, we may assume P is primitive. We easily verify that the desired inequality holds if P is a rotation of one of the grid polygons in Figure 3.1; hence, let us assume that this is not the case. Let α_m be the number of m-cycles in π_P. We have

$$\frac{\mathrm{perim}(P)}{\mathrm{cyc}(P)} = \frac{3\alpha_3 + \sum_{m\geqslant 4} m\alpha_m}{\alpha_3 + \sum_{m\geqslant 4} \alpha_m}.$$

For fixed values of $\alpha_4, \alpha_5, \ldots$, the function $x \mapsto \dfrac{3x + \sum_{m\geqslant 4} m\alpha_m}{x + \sum_{m\geqslant 4} \alpha_m}$ is decreasing in x whenever $x \geqslant 0$. Therefore, we can apply Lemma 3.3 to find that

$$\frac{\mathrm{perim}(P)}{\mathrm{cyc}(P)} \geqslant \frac{3(\alpha_4 + \sum_{m\geqslant 5}(m-2)\alpha_m) + \sum_{m\geqslant 4} m\alpha_m}{(\alpha_4 + \sum_{m\geqslant 5}(m-2)\alpha_m) + \sum_{m\geqslant 4} \alpha_m} = \frac{7\alpha_4 + \sum_{m\geqslant 5}(4m-6)\alpha_m}{2\alpha_4 + \sum_{m\geqslant 5}(m-1)\alpha_m}.$$

Since $4m-6 \geqslant \frac{7}{2}(m-1)$ for all $m \geqslant 5$, we find that $\mathrm{perim}(P) \geqslant \frac{7}{2}\,\mathrm{cyc}(P) > \frac{7}{2}\,\mathrm{cyc}(P) - \frac{3}{2}$. □

We now proceed to prove Theorems 1.1 and 1.3. Recall that we have scaled the triangular grid so that each pane has length 1. Given a cycle c in π_P, we write $\mathrm{length}(\mathrm{traj}(c))$ for the *length* of $\mathrm{traj}(c)$, which is just the total length of the line segments in $\mathrm{traj}(c)$. It is easy to check that $\mathrm{area}(P) = \frac{2}{3}\sum_c \mathrm{length}(\mathrm{traj}(c))$, where the sum is over all cycles in π_P.

Proposition 3.4. *If P is a primitive grid polygon that is not a rotation of one of the grid polygons in Figure 3.1, then* $\operatorname{area}(P) \geqslant 6\operatorname{cyc}(P)$.

Proof. The proof is by induction on $\operatorname{area}(P)$. Because P is primitive, all of the triangular trajectories in the billiards system of P have length at least $15/2$. Let us first assume that every triangular trajectory in the billiards system of P has length strictly greater than $15/2$. This forces every triangular trajectory to have length at least $21/2$. Because P is primitive, every line segment in a trajectory in the billiards system of P has length at least $3/2$. Therefore, $\operatorname{length}(\operatorname{traj}(c)) \geqslant 3m/2$ for every m-cycle c in π_P. It is also straightforward to check that every 4-cycle in π_P has a trajectory of length at least 9 and that every 5-cycle in π_P has a trajectory of length at least $21/2$. Let α_m denote the number of m-cycles in π_P. Because $\operatorname{area}(P) = \frac{2}{3}\sum_c \operatorname{length}(\operatorname{traj}(c))$ (with the sum ranging over all cycles in π_P), we have

$$\begin{aligned}\operatorname{area}(P) &\geqslant \frac{2}{3}\left((21/2)\alpha_3 + 9\alpha_4 + (21/2)\alpha_5 + \sum_{m\geqslant 6}(3m/2)\alpha_m\right)\\ &= 7\alpha_3 + 6\alpha_4 + 7\alpha_5 + \sum_{m\geqslant 6} m\alpha_m\\ &\geqslant 6\operatorname{cyc}(P).\end{aligned}$$

Now assume that the billiards system of P contains at least one triangular trajectory Δ of length $15/2$. Then up to rotation, P must have the following shape, where curvy curves are schematic illustrations of parts of the boundary of P:

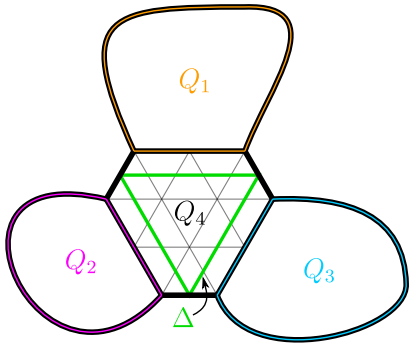

The polygon P consists of pieces Q_1, Q_2, Q_3, Q_4 as shown: the boundaries of Q_1, Q_2, Q_3 are indicated by thin orange, pink, and teal strips, respectively, and Q_4 is the closure of $P \setminus (Q_1 \cup Q_2 \cup Q_3)$. We also allow for each of Q_1, Q_2, Q_3 to be a single line segment with area 0 (a degenerate grid polygon). Because P is primitive, none of Q_1, Q_2, Q_3 can have area 1 or 2. If $\operatorname{area}(Q_i) \leqslant 3$ for all $i \in \{1,2,3\}$, then (because it is not a rotation of a polygon in Figure 3.1) P must be a rotation of one of the polygons

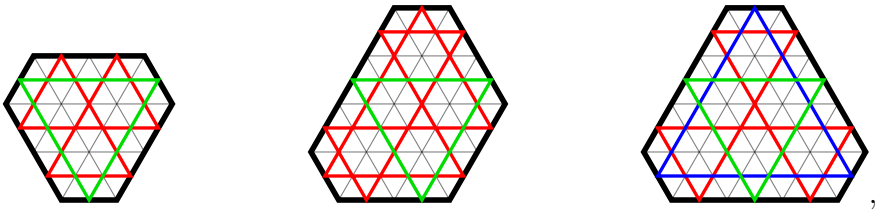

so we can check directly that $\operatorname{area}(P) \geqslant 6\operatorname{cyc}(P)$. Hence, we may suppose that $\operatorname{area}(Q_i) \geqslant 4$ for some $i \in \{1,2,3\}$; without loss of generality, assume $\operatorname{area}(Q_1) \geqslant 4$. Let $Q' = Q_2 \cup Q_3 \cup Q_4$. Our strategy is to invoke Lemma 3.1 with $P_1 = Q_1$ and $P_2 = Q'$. With these choices of P_1 and P_2, let δ_1 and δ_2 be as defined in Lemma 3.1.

Let t_1 and t_2 be the unique panes in the boundary of Q_1 that touch the boundary of Q' but are not contained in Q'. Because P is primitive and Q_1 has area at least 4, there are eight possibilities for the orientations of t_1 and t_2; these possibilities are depicted in Figure 3.2.

Suppose first that the orientations of t_1 and t_2 are as shown in one of the four images on the top of Figure 3.2. Then Q_1 is primitive. If Q_1 is not a rotation of one of the grid polygons in Figure 3.1, then we may apply induction to see that

$$\operatorname{area}(Q_1) \geqslant 6\operatorname{cyc}(Q_1) \geqslant 6(\operatorname{cyc}(Q_1) - \delta_1 + 1).$$

On the other hand, if Q_1 is a rotation of one of the polygons in Figure 3.1, then it must be a rotation of the rightmost polygon in that figure. In this case, $\operatorname{area}(Q_1) = 16$, $\operatorname{cyc}(Q_1) = 3$, and $\delta_1 = 2$, so $\operatorname{area}(Q_1) \geqslant 6(\operatorname{cyc}(Q_1) - \delta_1 + 1)$ again.

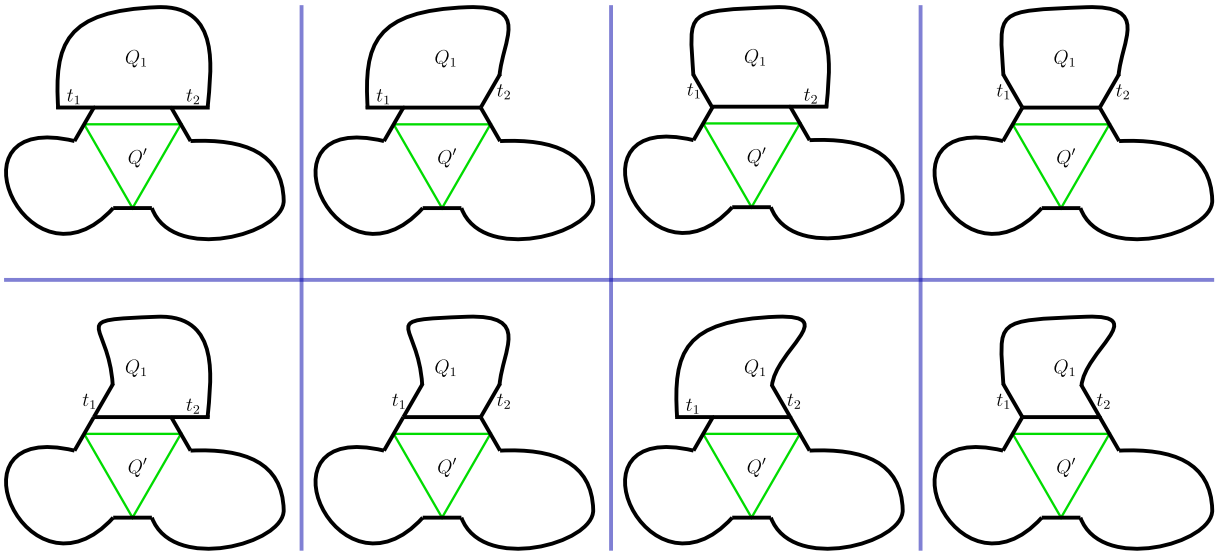

Figure 3.2: The eight possible orientations of the panes t_1 and t_2.

Now suppose the orientations of t_1 and t_2 are as shown in one of the four images on the bottom of Figure 3.2. In this case, we have $Q_1 = \widetilde{Q}_1 \cup T$, where T is a grid polygon that is a triangle of area 1 and $\widetilde{Q}_1 \cap T$ is a single pane. In the two left (respectively, right) images on the bottom of Figure 3.2, the triangle T has t_1 (respectively, t_2) as one of its sides. Note that $\widetilde{Q}_1$ is primitive. It follows from Corollary 3.2 that $\operatorname{cyc}(\widetilde{Q}_1) = \operatorname{cyc}(Q_1)$. If $\widetilde{Q}_1$ is not a rotation of one of the grid polygons in Figure 3.1, then we can use induction to see that

$$\operatorname{area}(\widetilde{Q}_1) \geqslant 6\operatorname{cyc}(\widetilde{Q}_1) = 6\operatorname{cyc}(Q_1) \geqslant 6(\operatorname{cyc}(Q_1) - \delta_1 + 1).$$

On the other hand, if $\widetilde{Q}_1$ is a rotation of one of the polygons in Figure 3.1, then (because $\operatorname{area}(\widetilde{Q}_1) \geqslant 3$) it is straightforward to check that $\delta_1 = 2$ and that $\operatorname{area}(Q_1) \geqslant 6(\operatorname{cyc}(Q_1) - 1)$. Thus, $\operatorname{area}(Q_1) \geqslant 6(\operatorname{cyc}(Q_1) - \delta_1 + 1)$ in this case as well.

We have shown that in each of the eight possible cases illustrated in Figure 3.2, we have

$$\operatorname{area}(Q_1) \geqslant 6(\operatorname{cyc}(Q_1) - \delta_1 + 1). \tag{3.1}$$

Now, Q' is primitive, and it is clearly not a single triangle of area 1 or a unit hexagon. Invoking Lemma 3.1 with $P_1 = Q_1$, $P_2 = Q'$, and $\eta = 2$, we find that

$$\operatorname{cyc}(P) \leqslant \operatorname{cyc}(Q_1) + \operatorname{cyc}(Q') - \delta_1 - \delta_2 + 2 \leqslant (\operatorname{cyc}(Q_1) - \delta_1 + 1) + \operatorname{cyc}(Q').$$

If Q' is not a rotation of one of the polygons in Figure 3.1, then we can use induction to see that $\operatorname{area}(Q') \geqslant 6\operatorname{cyc}(Q')$. In this case, we can apply (3.1) to see that

$$\operatorname{area}(P) = \operatorname{area}(Q_1) + \operatorname{area}(Q') \geqslant 6((\operatorname{cyc}(Q_1) - \delta_1 + 1) + \operatorname{cyc}(Q')) \geqslant 6\operatorname{cyc}(P),$$

as desired. On the other hand, if Q' is a rotation of one of the polygons in Figure 3.1, then it is a rotation of the rightmost such polygon, so $\operatorname{area}(Q') = 16$, $\operatorname{cyc}(Q') = 3$, and $\delta_2 = 2$. In this case,

$$\operatorname{cyc}(P) \leqslant \operatorname{cyc}(Q_1) + \operatorname{cyc}(Q') - \delta_1 - \delta_2 + 2 = \operatorname{cyc}(Q_1) + 3 - \delta_1,$$

so invoking (3.1) yields

$$\operatorname{area}(P) = \operatorname{area}(Q_1) + 16 \geqslant 6(\operatorname{cyc}(Q_1) - \delta_1 + 1) + 16 > 6(\operatorname{cyc}(Q_1) + 3 - \delta_1) \geqslant 6\operatorname{cyc}(P),$$

as desired. □

With the previous proposition out of the way, we can painlessly finish proving Theorems 1.1 and 1.3. Let us first establish one additional piece of terminology. Let P be a grid polygon. It is possible to find a sequence $(P_k)_{k=1}^r$ of grid polygons and a sequence $(Q_k)_{k=1}^r$ of primitive grid polygons with $P_1 = Q_1$ and $P = P_r$ such that $P_k = P_{k-1} \cup Q_k$ and such that $P_{k-1} \cap Q_k$ is a single pane for all $k \in \{2, \dots, r\}$. Moreover, the primitive grid polygons $Q_1, \dots, Q_r$ are uniquely determined up to reordering. We call $Q_1, \dots, Q_r$ the *primitive pieces* of P.

Proof of Theorems 1.1 and 1.3. Let $Q_1, \dots, Q_r$ be the primitive pieces of P. For each $i \in [r]$, Proposition 3.4 tells us that $\operatorname{area}(Q_i) \geqslant 6\operatorname{cyc}(Q_i)$ if Q_i is not a rotation of one of the grid polygons in Figure 3.1; if Q_i *is* a rotation of one of the grid polygons in Figure 3.1, then we can check directly that $\operatorname{area}(Q_i) \geqslant 6\operatorname{cyc}(Q_i) - 6$. It follows from Corollary 3.2 that $\operatorname{cyc}(P) = \sum_{i=1}^r \operatorname{cyc}(Q_i) - (r-1)$. Thus,

$$\begin{aligned}
\operatorname{area}(P) &= \sum_{i=1}^r \operatorname{area}(Q_i) \\
&\geqslant \sum_{i=1}^r (6\operatorname{cyc}(Q_i) - 6) \\
&= 6\left(\sum_{i=1}^r \operatorname{cyc}(Q_i) - (r-1)\right) - 6 \\
&= 6\operatorname{cyc}(P) - 6.
\end{aligned}$$

This completes the proof of Theorem 1.1. This argument shows that $\mathrm{area}(P) = 6\,\mathrm{cyc}(P) - 6$ if and only if $\mathrm{area}(Q_i) = 6\,\mathrm{cyc}(Q_i) - 6$ for all $i \in [r]$. By invoking Proposition 3.4 and inspecting the grid polygons in Figure 3.1, we see that this occurs if and only if the primitive pieces $Q_1, \ldots, Q_r$ are all unit hexagons. This proves Theorem 1.3. □

4. Reflections and next directions

We believe that this article just scratches the surface of rigid combinatorial billiards systems and their connections with plabic graphs and membranes. In this section, we discuss several variations and potential avenues for future research.

4.1. Perimeter vs. cycles

Recall Conjecture 1.4, which says that $\mathrm{perim}(P) \geqslant 4\,\mathrm{cyc}(P) - 2$ for every grid polygon P. The grid polygons P satisfying $\mathrm{perim}(P) = 4\,\mathrm{cyc}(P) - 2$ seem more sporadic and unpredictable than the equality cases of Theorem 1.1, which are just the trees of unit hexagons by Theorem 1.3. This gives a heuristic hint as to why Conjecture 1.4 is more difficult to prove than Theorem 1.1.

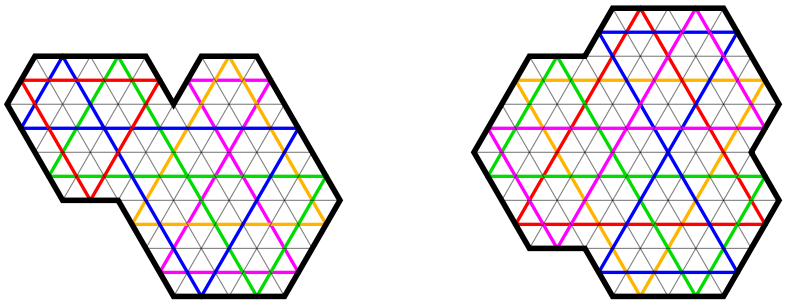

Figure 4.1: Two grid polygons with perimeter 18, each of which has 5 cycles in its billiards system.

4.2. Other families of plabic graphs

Let G be a connected reduced plabic graph with n marked boundary points and v vertices, and let c be the number of cycles in the trip permutation π_G. Corollary 1.6 provides inequalities that say how large n and v must be relative to c in the case when G has essential dimension 2. One can ask for similar inequalities when G is taken from some other interesting family of plabic graphs. One natural candidate for such a family is the collection of plabic graphs of essential dimension 3; we refer to [LP20] for further details concerning the definition. It is also natural to consider plabic graphs that can be obtained from polygons in other planar grids besides the triangular grid; Figure 4.2 shows some examples (in these examples, we dismiss our earlier assumption that all vertices in a plabic graph are trivalent).

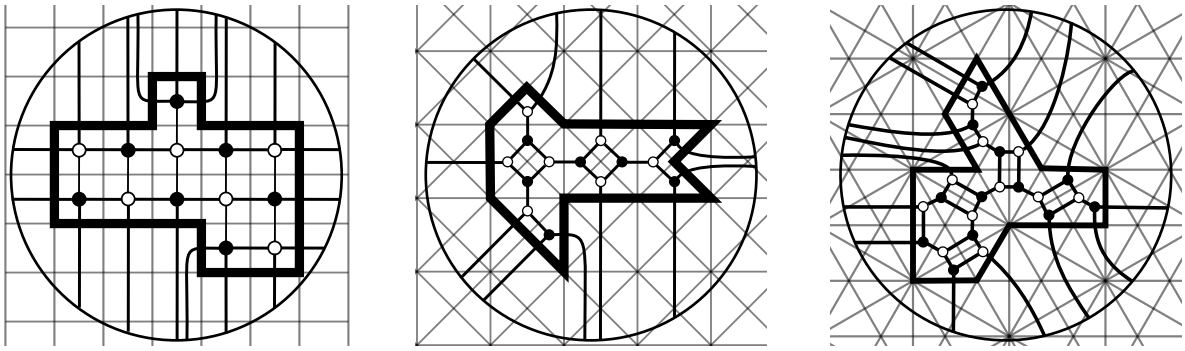

Figure 4.2: Plabic graphs obtained from polygons in different planar grids.

If G is a plabic graph obtained from the square grid (as on the left of Figure 4.2), then it is not too difficult to prove that $v \geqslant 3c - 2$ and that $n \geqslant 4c$; moreover, these bounds are tight. We omit the details.

4.3. Regions with holes

Suppose Q is a region in the triangular grid obtained from a grid polygon by cutting out some number of polygonal holes. We can define the billiards system for Q in the same way that we defined it for a grid polygon. It would be interesting to obtain analogues of Theorems 1.1, 1.2, 1.3, and 1.5 in this more general setting. The resulting analogues of Theorems 1.1 and 1.2 might need to incorporate the genus of Q. Indeed, Figure 4.3 shows a region Q with genus 1 for which the inequalities in Theorems 1.1 and 1.2 are false as written.

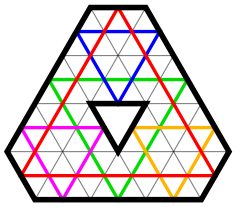

Figure 4.3: Trajectories in a triangular grid region of genus 1.

Acknowledgements

We are grateful to Alex Postnikov for helpful conversations. We thank Noah Kravitz for suggesting that we consider billiards systems in square grids and in triangular grid regions with holes cut out, as discussed in Section 4. We thank the anonymous referee for helpful suggestions.

References

[AHBC+16] Nima Arkani-Hamed, Jacob Bourjaily, Freddy Cachazo, Alexander Goncharov, Alexander Postnikov, and Jaroslav Trnka. *Grassmannian geometry of scattering amplitudes*. Cambridge University Press, Cambridge, 2016. doi:10.1017/CBO9781316091548.

[BKM78] Carlo Boldrighini, Michael Keane, and Federico Marchetti. Billiards in polygons. *Ann. Probab.*, 6(4):532–540, 1978.

[CFG91] Hallard T. Croft, Kenneth J. Falconer, and Richard K. Guy. Billiard ball trajectories in convex regions. In *Unsolved Problems in Geometry*. Springer–Verlag, New York, 1991.

[CSD63] H. T. Croft and H. P. F. Swinnerton-Dyer. On the Steinhaus billiard table problem. *Proc. Cambridge Philos. Soc.*, 59:37–41, 1963. doi:10.1017/s0305004100001961.

[DR83] Duane DeTemple and Jack Robertson. Permutations associated with billiard paths. *Discrete Math.*, 47(2-3):211–219, 1983. doi:10.1016/0012-365X(83)90091-2.

[DR85] Duane W. DeTemple and Jack M. Robertson. Convex Curves with Periodic Billiard Polygons. *Math. Mag.*, 58(1):40–42, 1985.

[FPST22] Sergey Fomin, Pavlo Pylyavskyy, Eugenii Shustin, and Dylan Thurston. Morsifications and mutations. *J. Lond. Math. Soc. (2)*, 105(4):2478–2554, 2022. doi:10.1112/jlms.12566.

[Gar84] Martin Gardner. Bouncing balls in polygons and polyhedrons. In *The Sixth Book of Mathematical Games from Scientific American*. University of Chicago Press, Chicago, IL, 1984.

[GPW22] Pavel Galashin, Alexander Postnikov, and Lauren Williams. Higher secondary polytopes and regular plabic graphs. *Adv. Math.*, 407:Paper No. 108549, 52, 2022. doi:10.1016/j.aim.2022.108549.

[Gut86] Eugene Gutkin. Billiards in polygons. *Phys. D*, 19(3):311–333, 1986. doi:10.1016/0167-2789(86)90062-X.

[Hal77] Benjamin Halpern. Strange billiard tables. *Trans. Amer. Math. Soc.*, 232:297–305, 1977. doi:10.2307/1998942.

[KW14] Yuji Kodama and Lauren Williams. KP solitons and total positivity for the Grassmannian. *Invent. Math.*, 198(3):637–699, 2014. doi:10.1007/s00222-014-0506-3.

[LP20] T. Lam and A. Postnikov. Polypositroids. 2020. arXiv:2010.07120.

[LPW20] Tomasz Lukowski, Matteo Parisi, and Lauren K. Williams. The positive tropical Grassmannian, the hypersimplex, and the $m = 2$ amplituhedron. 2020. arXiv:2002.06164.

[Pos06] A. Postnikov. Total positivity, Grassmannians, and networks. 2006. arXiv:math/0609764.

[PSBW21] Matteo Parisi, Melissa Sherman-Bennett, and Lauren K. Williams. The $m = 2$ amplituhedron and the hypersimplex: signs, clusters, triangulations, Eulerian numbers. 2021. arXiv:2104.08254.

[SK79] Robert Sine and Vladislav Kreĭnovič. Remarks on billiards. *Amer. Math. Monthly*, 86(3):204–206, 1979. doi:10.2307/2321524.

[STWZ19] Vivek Shende, David Treumann, Harold Williams, and Eric Zaslow. Cluster varieties from Legendrian knots. *Duke Math. J.*, 168(15):2801–2871, 2019. doi:10.1215/00127094-2019-0027.